Published in final edited form as:
Traffic. 2012 May ; 13(5): 727–744. doi:10.1111/j.1600-0854.2012.01343.x.

Electron Tomography Reveals Rab6 Is Essential to the Trafficking of *trans*-Golgi Clathrin and COPI-Coated Vesicles and the Maintenance of Golgi Cisternal Number

Brian Storrie[*,#], **Massimo Micaroni**[†], **Garry P. Morgan**[†], **Nick Jones**[*], **Jeffrey A. Kamykowski**[*], **Ngozi Wilkins**[*], **Timothy H. Pan**[†], and **Brad J. Marsh**[†,‡,§,‖]

[*]Department of Physiology and Biophysics, University of Arkansas for Medical Sciences, Little Rock, AR 72205, USA

[†]Institute for Molecular Bioscience, The University of Queensland, St Lucia, QLD 4072, Australia

[‡]Centre for Microscopy & Microanalysis, The University of Queensland, St Lucia, QLD 4072, Australia

[§]ARC Centre of Excellence in Bioinformatics, The University of Queensland, St Lucia, QLD 4072, Australia

[‖]School of Chemistry & Molecular Biosciences, The University of Queensland, St Lucia, QLD 4072, Australia

Abstract

We have shown previously that Rab6, a small, *trans*-Golgi-localized GTPase, acts upstream of the COG and ZW10/RINT1 retrograde tether complexes to maintain Golgi homeostasis. Here, we present evidence from the unbiased and high-resolution approach of electron microscopy and electron tomography that Rab6 is essential to the *trans*-Golgi trafficking of two morphological classes of coated vesicles; the larger corresponds to clathrin-coated vesicles and the smaller to COPI-coated vesicles. Based on the site of coated vesicle accumulation, cisternal dilation, and the normal kinetics of cargo transport from the ER to Golgi followed by delayed Golgi to cell surface transport, we suggest that Golgi function in cargo transport is preferentially inhibited at the t*rans*-Golgi/TGN. The >50% increase in Golgi cisternae number in Rab6-depleted HeLa cells that we observed may well be coupled to the trans-Golgi accumulation of COPI-coated vesicles; depletion of the individual Rab6 effector, myosin IIA, produced an accumulation of uncoated vesicles with if anything a decrease in cisternal number. These results are the first evidence for a Rab6-dependent protein machine affecting Golgi-proximal, coated vesicle accumulation and likely transport at the *trans*-Golgi and the first example of concomitant cisternal proliferation and increased Golgi stack organization under inhibited transport conditions.

Keywords

Rab6; Golgi cisternae; membrane traffic; transport vesicles; VSV-G; myosin II; HeLa cells; electron microscopy; electron tomography; 3-dimensional reconstruction

[#]Corresponding author: StorrieBrian@uams.edu; Tel: (501) 526-7418; Fax: (501) 686-8167.

Supplementary Data

Multimedia files generated as *QuickTime*® movies from sets of TIF/PNG images captured directly from tomographic data using the *3dmod viewer* in *IMOD* are provided to accompany the figure panels for figures 4, 5, 7 and 9.

INTRODUCTION

Of the 12 different Golgi associated Rab proteins (for review, see 1), small GTPases of the Rab family, Rab6 is the most abundant (2). It consists of 4 different isoforms, Rab6a, Rab6a', Rab6b and Rab6c (for review, see 3 and also 4–6). Of these, Rab6a and Rab6a' which are equally abundant and differ in 3 amino acids are the only family members expressed in all cell types of the mammalian body. Rab6b is neuronal specific (4) while Rab6c is expressed in a limited number of human tissues and is involved in cell cycle progression (7). Rab6a and Rab6a' are preferentially localized to the *trans*-Golgi cisterna/*trans*-Golgi network (TGN) while other Golgi associated Rabs exhibit different localizations with Rab1 and Rab2, for example, preferentially localized to the *cis*-Golgi apparatus/*cis*-Golgi network.

Like all Rab proteins Rab6a and Rab6a' function as molecular switches that regulate membrane trafficking and organelle organization in diverse ways. In the GTP-bound state, they are both associated with *trans*-Golgi membranes and are active in effector recruitment. To date more than 15 individual Rab6a/a' effectors have been identified (for review, see 8). These include a series of motor proteins and/or motor protein regulators such as myosin II, KIF1C, KIF5B and at least 4 different members of the golgin family of coiled coil proteins, GCC185, golgin 97, TMF and OCRL. With the exception of Rabkinesin 6, a mitotic kinesin (aka Rab6-KIFL/MKlp2/KIF20A), little, if any, evidence exists to suggest a differential interaction of any of the other effectors with Rab6a versus Rab6a' and, in fact, considerable, but not all evidence suggests that the two closely related isoforms are functionally redundant. How Rab6a/a' can produce the contextual sensitive recruitment of these effectors or balance the relative importance of individual effectors to maintain Golgi homeostasis remain open questions. For the sake of simplicity, we shall refer to Rab6a and Rab6a' collectively as Rab6. This convention is consistent with the original naming of Rab6a as Rab6 as this was the first discovered member of this Rab subfamily.

In previous work, we found that Rab6 knockdown suppressed Golgi fragmentation and vesicle dispersal in HeLa cells depleted of the retrograde Golgi tether proteins, ZW10/RINT1 and Conserved Oligomeric Golgi complex (COG), in particular the COG3 subunit (9). In a formal genetic sense, this outcome strongly indicates that Rab6 is acting upstream of both the ZW10/RINT1 and COG complexes. One plausible common mechanism follows from the fact that these tether systems are important to vesicular trafficking, albeit at different stages. If Rab6 acted to recruit motor proteins important to the Golgi-proximal movement of either set of vesicles, then in the absence of normal vesicle movement and consumption there might well be a feedback inhibition of vesicle budding and hence Golgi fragmentation. Any unbalancing of membrane trafficking under these conditions might well have profound affects on Golgi cisternal homeostasis.

In the present work, we tested in HeLa cells several predictions of this hypothesis. First, we predicted that with Rab6 depletion that *trans*-Golgi proximal vesicles would accumulate and because of possible feedback effects there would a concomitant accumulation of arrested *trans*-Golgi vesicle budding structures. Second, we predicted that decreased trafficking might well lead to increased cisternal continuity. Vesicle budding is normally thought to limit cisternal continuity. Third, we predicted that the depletion of Rab6 as a *trans*-Golgi protein might well unbalance Golgi membrane trafficking such that there would be little, if any, inhibition of endoplasmic reticulum (ER) to Golgi trafficking, but a pronounced inhibition of Golgi to plasma membrane trafficking. If so, in accordance with a cisternal maturation model, the number of cisternae per Golgi stack might well increase. We used VSV-G protein transport from the ER to plasma membrane as independent assay for cargo transport. Fourth, we tested the prediction that the depletion of a single Rab6 effector,

myosin II recently shown to be involved in vesicle formation at the TGN, would mimic the central elements of this hypothesis. Because vesicle accumulation should be Golgi proximal, we took as the major experimental readout in our experiments electron microscopy and in particular electron tomography where a full 3-dimensional imaging of vesicle structure and size could be established.

The net outcome of these experiments was to place Rab6 as a *trans*-Golgi specific factor in coated vesicle budding/vesicle consumption. The finding that the vesicles were coated was both novel and unexpected. All previous evidence had indicated a role for Rab6 in coat-free vesicle trafficking (10,11). Coated-vesicle accumulation in Rab6-depleted cells was accompanied by increased cisternal continuity and cisternal number with effects on cargo transport from the ER to plasma membrane being specific to the Golgi apparatus/TGN. Contrary to expectation, myosin I I-depletion did not mimic the Rab6 knockdown phenotype as revealed by electron microscopy. In fact, the myosin II depletion phenotype displayed in electron micrographs was not a noticeable aspect of the Golgi structure in Rab6 knockdown cells. In sum, we conclude that Rab effectors are not created equal in phenotypic importance to Golgi organization and suggest that the most phenotypically critical Rab6-dependent step(s) affects the transport of Golgi coated vesicles of which at least a portion morphologically identified as COPI-coated vesicles are likely intra-Golgi retrograde carriers.

RESULTS

We hypothesized based on our previous results (9) that Rab6 is an important regulator of Golgi associated vesicle trafficking/transport. If so, we speculated that many of these events are Golgi proximal and hence below the 200 nm resolution of light microscopy. Therefore, we employed the higher resolution approach of electron microscopy. In our initial experiments, we used two different siRNAs to Rab6. Both are directed against nucleotide sequences common to Rab6a/a' mRNA and effectively knockdown both protein isoforms. We refer to the first as siRab6(Sun) and the second as siRab6(Young). The two siRNAs were independently validated in parallel experiments by Sun et al. (9) and Young et al. (12). As shown in Figure 1 when cells were treated with either of these two siRNAs for 4 d, the Golgi apparatus in thin sections of chemically fixed HeLa cells appeared expanded with a proliferation of cisternae that often exhibited substantial dilation (compare Figure 1A (Control) and Figure 1B, C) and an accumulation of coated membrane profiles (arrowheads). The two siRNAs directed against Rab6 produced equivalent morphologic effects. As expected for the equivalent morphological phenotype, each siRab6 produced an equivalent concentration dependent knockdown of Rab6 protein (Figure 1D–F). Based on this demonstrated equivalency, we chose in all subsequent experiments to use siRab6(Sun), the siRNA previously characterized by this laboratory.

Thin Section Electron Microscopy Indicates that Rab6 Regulates Golgi Proximal Coated Vesicle Trafficking and Golgi Structure

We reasoned that much of the cisternal dilation observed with Rab6 knockdown was an artifact of the chemical fixation procedure. Hence, we tested high pressure freezing followed by freeze substitution as an alternate state-of-the-art approach to sample preparation. High pressure freezing has the advantage of holding in place cellular structures within 10 msec. When HeLa cells treated with nonsense siRNA (siControl, 9) and high pressure frozen were examined in thin section electron micrographs, the Golgi apparatus appeared similar in profile to that observed in chemically fixed cells (compare Figure 1A and Figure 2A) indicating both roughly comparable sample preservation and that the siRNA protocol itself did not induce any detectable non-specific changes to Golgi structure. This conclusion is consistent with previous light microscopy (9). On average, individual Golgi stacks were

comprised of ~4 cisternae, and there were a relatively small number of 'free' vesicles and/or budding vesicle profiles associated with the Golgi ribbon or with the membranes of Golgi cisternae, respectively (see, Figure 2A, asterisk and inset).

In contrast, high pressure freezing was essential to preserving the morphological features of the Rab6-depleted Golgi (Figure 2B,C). Rather than appearing as an often fragmented and generally dilated structure (Figure 1B,C), the Golgi apparatus in Rab6-depleted cells following high pressure freezing appeared as long continuous cisternae with any dilated, swollen structures restricted to 1 to 2 cisternae at one side of the Golgi stack (Figure 2B). These better preserved Golgi profiles showed significant qualitative and quantitative differences in Golgi organization as well as vesicle arrangement compared to controls. In some cases, Golgi cisternae appeared to be de-adhered (Figure 2B, arrowhead) and 2-dimensional imaging of thin sections by electron microscopy revealed a significant increase (~15-fold) in the number of vesicular 'budding profiles' that remained either continuous with or directly attached/tethered to Golgi cisternae (Figure 2B; see also later Figures). The morphological appearance of these extensive 'budding' profiles appeared to represent vesicles which had successfully formed via established coat-mediated mechanisms (13), as indicated by the presence of electron dense protein coats and size (Figure 2B, insets) consistent with previous morphological studies (14–17). We refer to the 'budding' profiles by the neutral term of Ω figures as arrested budding versus fusion can not be determined from a single time point. The coat associated with the larger vesicle profiles had the spiked appearance typical of clathrin, in accordance with previous detailed characterization at the electron microscope level in high-pressure frozen mammalian cells (Figure 1B, asterisk, left inset) (14,15,17) and exhibited a polarized distribution relative to the *cis*-*trans* axis, i.e., these apparent clathrin coated Ω figures were primarily distributed to the *trans*-face of the stacks/ribbon. We assigned the dilated cisternae associated with these larger profiles as *trans*-cisternae/TGN. Interestingly, arrested, larger Ω figures were found not only at periphery of *trans*-cisternal membranes but also laterally along their length when Golgi cisternae were not in close apposition (Figure 2B, asterisk, left inset). Similarly, in areas of the ribbon where medial-cisternae were not positioned immediately adjacent to one another, smaller, presumably COPI-coated arrested profiles were observed (Figure 2B, arrowhead, right inset). Together, these results strongly indicate that Rab6 regulates coated vesicle dynamics at the mammalian Golgi. This is a surprising outcome because Rab6 has been previously implicated in coated vesicle-independent trafficking (e.g., 10).

A third key finding was that the number of cisternae per Golgi stack was reproducibly increased in thin sectioned Rab6 knockdown cells relative to controls (6.8 ± 0.46 versus 4.2 ± 0.32 cisternae per stack, respectively), with up to 9 individual cisternae found within a single stack in some instances, as highlighted in the example shown in Figure 2B. Fourth, the linear continuity of the Golgi's ribbon-like architecture in Rab6-depleted cells was significantly increased compared to control cells (e.g. compare Figure 2A and 2B). We suggest that the increases observed for the number of stacked cisternae as well as lateral continuity along the length of the Golgi ribbon may result indirectly from the inhibition of efficient vesicle trafficking from Golgi cisternae combined with effects on lateral cisternal fusion. Previous ultrastructural studies which have examined the changes that result from incubating mammalian cells at 20°C to block the exit of protein cargo from the Golgi have only reported increases in the size of *trans*-cisternae/TGN as a consequence of arresting the exit of membrane traffic from the Golgi (17–21), in contrast to the significant changes in cisternal number and continuity that we report here.

Since our analysis of coated vesicle profiles by electron microscopy of thin sections prepared from Rab6-depleted HeLa cells indicated a polarized distribution vertically across Golgi stacks, we predicted that Golgi glycosyltransferases/resident proteins should also

maintain a polarized distribution relative to the *cis-trans* axis. Subsequent confocal immunofluorescence images of the *cis*-Golgi marker, p115, and β-galactosyltransferase (GalT, a glycosyltransferase preferentially distributed to *trans*-Golgi cisternae) clearly demonstrated that these two markers could be readily distinguished from one another in both siControl- and siRab6-treated cells (Figure 3, A and B), thus providing strong evidence confirming that fundamental Golgi organization remained intact for HeLa cells in which Rab6 knockdown was high (Figure 2C); similar results obtained by indirect immunofluorescence labeling of a second pair of *cis*- and *trans*-markers (gpp130 and TGN46, respectively) further confirmed the polarized distribution of these Golgi proteins in Rab6-depleted cells (data not shown). Furthermore, in many cases the extent of increased lateral continuity along the ribbon in Rab6 knockdown cells was striking relative to controls even at the light microscope level (Figure 3B *versus* Figure 3A). By immunogold labeling, we found the relative distribution of GalNAcT2-GFP across the Golgi stack to be unaltered with Rab6-depletion (Micaroni and Marsh, unpublished observations).

Electron Tomography Validates a Role for Rab6 in the Dynamics of Free Coated Vesicles and Golgi Homeostasis

Although thin section analysis (Figure 1 and 2) suggested a Rab6-dependent inhibition of vesicle dynamics in siRab6 cells, the limitations of conventional 2-dimensional analysis by electron microscopy prevented an unambiguous quantification of the size or number of apparent vesicles and Ω figure profiles. The combination of fast, high pressure-freezing/ freeze-substitution fixation with high-resolution electron tomography has previously shown that Golgi-associated vesicles can be reliably classified as either clathrin- or COPI-coated structures according to the combination of their coat thickness/morphology and size (14,15,22,23). In addition, high-resolution 3-dimensional reconstructions of the Golgi region generated by electron tomography afforded more robust quantitative analysis of the structure of the Golgi and its component cisternae than could ever be achieved by attempting to extrapolate its 3-dimensional organization from 2-dimensional micrographs (23–30). Consequently, we used cellular electron tomography to image then reconstruct thick (i.e. 300 nm) sections encompassing representative Golgi regions. The tomographic slice presented in Figure 4A (see also Fig 4A tomo.mov) - taken from the mid-plane (in Z) of a 3-dimenional reconstruction of the Golgi region in a control HeLa cell - highlights the basic hallmarks of ‘normal’ Golgi organization in mammalian cells: individual stacks of Golgi cisternae (compact regions) situated in relatively close proximity to one another, together forming a larger ribbon-like structure that extends laterally (24,31–33). Consistent with 2-dimenional images of thin sections (Figure 2A), 3-dimensional analysis of tomographic reconstructions confirmed that each stack contained ~4 cisternae on average, accompanied by a relatively small number of vesicles (Table 1). Further, microtubules were present within the Golgi region of control cells (Figure 4B, see also Fig 4B model.mov).

As well as using coat appearance as a putative marker for the *trans*-Golgi, the direct physical juxtaposition of ER membranes with *trans*-cisternae in electron tomograms provided an additional means of reliably assessing each stack’s polarity in accordance with previous studies (14,17,24,28,34–36) (Figure 4A, inset). Using these two criteria, individual cisternae were segmented and color-coded according to the polarity of each stack and surface-rendered models were then generated for unambiguous 3-dimensional visualization of Golgi organization and for subsequent quantitative analysis (Figure 4, B and C). Detailed examination of the Golgi ribbon in tomograms of siControl cells revealed that individual stacks within the volume were for the most part spatially/structurally distinct from each other and only a small number of vesicles were found in the vicinity of the Golgi. In the example shown here, only 5 vesicles (3 clathrin, 2 COPI) were present (Figure 4D); a single COPI-coated Ω figure profile was also found. In contrast, a comparable representative

volume centered on the Golgi region in a Rab6-depleted cell revealed Golgi stacks that contained up to 7 cisternae (not including either the *cis*-most cisterna/CGN or the *trans*-most cisterna/TGN (Figure 5A, see also Fig 5A tomo.mov). Further, the dimensions of cisternae within individual Golgi stacks in Rab6-depleted cells were significantly larger than their counterparts in siControl cells both vertically (0.323 μm versus 0.229 μm) and laterally (3.272 μm versus 0.445 μm); in sum, stacked Golgi cisternae in siRab6 cells were larger in width, length and more numerous than in control HeLa cells. Quantitative differences were observed in multiple tomograms from individual cells (Table 1, e.g., 1.3x increase in stack width, 3.2 increase in cisternal length, and 1.51-fold increase in cisternal number on average).

In Rab6-depleted cells, the *trans*-most cisternae/TGN was considerably enlarged in Rab6-depleted cells compared to that in controls (Figure 5, A–C). This finding is consistent with the accumulation of Golgi vesicles along cisternal membranes. Of the 88 vesicular profiles associated with Golgi cisternae in the tomogram volume, 34 were clathrin-coated based on morphology and 54 were COPI-coated (see Figure A, insets for examples). Note that electron tomography permitted the assessment of coat morphology for each and every structure at various positions and angles within the tomogram. In either case (Figure 5A, insets; Figure 5, B and C, models; see also Fig 5 model.mov), physically continuous with Golgi cisternal membranes represented the majority of clathrin- or COPI-positive structures/vesicles identified (75% for clathrin versus 57% for COPI). In line with the original concept of ‘vesicles on strings’ (37) and consistent with our previous studies in insulin-secreting cells (16), COPI- and clathrin-coated ‘free’ vesicles in the Golgi region were located immediately proximal to cisternal membranes at the *cis*- and *trans*-Golgi, respectively (Figure 5, B–D). Likewise, the dimensions (Figure 5E) of both vesicle populations (identified and classified first on the basis of coat appearance) were consistent with previous measurements for clathrin and COPI vesicles in a variety of mammalian cell types prepared using a similar high-pressure freezing approach (14,15,17,27). Clathrin- and COPI-positive ‘free’ vesicles measured were 78.1 ± 2.6 nm and 47.4 ± 1.2 nm, respectively; clathrin- and COPI-positive cisternal continuous structures measured 70.4 ± 2.0 nm versus 45.4 ± 1.4 nm). The cisternal continuous Ω figures similarly fell into two size classes.

The significant accumulation of Golgi vesicles and Ω figure profiles, near doubling of the number of cisternae per stack and significant increase in cisternal length/continuity that followed Rab6-depletion suggested that the Golgi in these cells may be less dynamic relative to controls, particularly in light of evidence for direct and indirect roles for Rab6 in regulating microtubule binding and/or membrane recycling at the mammalian Golgi (12,38). To examine whether the Golgi remained sensitive to perturbations of the microtubule cytoskeleton, we tested the stability of the Golgi ribbon in siRab6 versus siControl cells in response to the microtubule-depolymerizing agent, nocodazole. Qualitatively, the pattern of scattered Golgi elements was similar (Figure 6, A, and B). Quantitatively, there was a small increase overall in nocodazole sensitivity suggesting the possibility of somewhat higher rates of Golgi recycling/transport in the Rab6-depleted cells (Figure 6C).

Finally, our electron microscope data provided evidence of a dramatic increase in the formation of expanded multivesicular bodies (MVB)/autophagic compartments in the vicinity of the Golgi region in Rab6 knockdown cells (Figure 7; see also Fig 7A′ tomo.mov, Fig 7B′ tomo.mov, Fig 7C tomo.mov). The presence within these compartments of different types of coated vesicles indicated an accumulation of transport intermediates as a consequence of Rab6 knockdown (Figure 7, white *versus* black arrows). These structures are likely autophagomes and/or intermediates in non-conventional secretion (39). Future studies will be required to determine fully the functional significance and mechanism of formation of these compartments. Of note the depletion of a Ypt6/Rab6 effector, the GARP complex,

leads to accumulation of autophagic structures in HeLa cells (40); in yeast, GARP/VFT mutants exhibit defective autophagy (41).

VSV-G Transport Is Inhibited Selectively by Rab6-Depletion at a Golgi to Plasma Membrane Stage but not at Earlier ER to Golgi Stage

Our electron microscopy analysis of the Golgi phenotype in Rab6 knockdown cells indicates an effect(s) that are particularly manifest at the *trans*-Golgi/TGN, i.e., *trans*-Golgi/TGN-specific cisternal dilation and accompanying coated Ω figures and vesicle accumulation. Moreover, the simplest explanation of the observed cisternal proliferation with Rab6 knockdown is based upon the predictions of the cisternal maturation model in which continued normal input from the ER coupled with inhibited export from the Golgi apparatus might well be result in a pronounced increase in cisternal number. Hence, we hypothesized that transport of the model cargo protein, VSV-G protein, from the ER to the plasma membrane should be normal from ER to Golgi, but inhibited at the level of Golgi to plasma membrane. As shown in Figure 8, this was exactly the outcome observed for the tsO45 temperature sensitive mutant of VSV-G protein that accumulates in the ER at 39.5°C and following temperature shift to 32°C then traffics via the Golgi apparatus to the plasma membrane. At the end of the 39.5°C ER accumulation period, the GFP tagged VSV-G mutant protein had accumulated in the ER as indicated by a web-like distribution of fluorescence across the cytoplasm in both Control (siScr) and siRab6(Sun) incubated wild type HeLa cells (Figure 8A). Cells were counterstained with Rab6 antibody to validate the level of Rab6 knockdown in each and every cell scored (data not shown). Upon shift to permissive conditions in the presence of cycloheximide to prevent further protein synthesis, VSV-G fluorescence accumulated juxtanuclearly in the Golgi region of the cell (Figure 8B). At the end of a 20 min chase at permissive temperature, 44 ± 4% of total VSV-G-GFP fluorescence was found juxtanuclearly in Control cells and 44 ± 5% in Rab6 depleted cells. From this, we conclude that the initial steps in VSV-G transport to the Golgi were unaffected by Rab6 depletion and hence are not Rab6-dependent.

To test whether Golgi to plasma membrane transport of VSV-G was affected by Rab6 depletion, we counterstained cells with a monoclonal antibody directed against an epitope present in the extracellular domain of VSV-G protein. In sum, each cell was characterized in 3 different fluorescence channels: total VSV-G distribution (VSV-G-GFP); cell surface VSV-G (extracellular domain epitope); and Rab6 level (rabbit antibodies directed against Rab6). As shown qualitatively in Figure 8B, surface appearance of VSV-G could be weakly detected for some Control cells as early as 40 min chase time while no surface appearance was detectable in siRab6 cells until a 90 min chase. When the intensity of surface VSV-G staining was quantified and averaged over a cell population, quantitatively significant surface accumulation of VSV-G at 60 min for Control cells and 90 min for siRab6 cells (Figure 8C). Even after a 120 min chase when the incidence of surface accumulation was high for both Control and siRab cells, there was still an approximately 2-fold lesser accumulation of VSV-G at the cell surface when the results were quantified and averaged across the scored cell population. Consistent with others (11,42), we conclude that Rab6 is a significant regulator of cargo transport to the plasma membrane. Based on our electron microscopy, this inhibition is likely to be at the *trans*-Golgi/TGN. Based on time-lapse microscopy, other investigators have concluded that the Rab6 effector, myosin IIA, is necessary for efficient vesicle formation and trafficking from the TGN (11).

Depletion of the Individual Rab6 Effector, Myosin IIA, Induces Extensive Golgi-Associated Vesicle Accumulation But Fails to Produce Increased Golgi Cisternal Number or Continuity

Myosin II and more specifically myosin IIA, MyoIIA, has been shown to be a Rab6 effector and a mediator of transport vesicle formation at the *trans*-Golgi apparatus (11,42). MyoIIA-dependent vesicles are required for efficient Golgi to plasma membrane transport and likely are uncoated (11,42). Hence MyoIIA depletion provides an excellent test of both the contribution of an individual effector to the Rab6 knockdown Golgi phenotype and how tightly coupled vesicle formation/transport to the plasma membrane and Golgi cisternal organization are. Using a siRNA directed against MyoIIA described by Miserey-Lenkei et al. (11), MyoIIA-depleted GalNAcT2-GFP HeLa cells were prepared for ultrastructural analysis in both 2-dimensions and 3-dimensions. Initial surveys of thin sections by electron microscopy revealed that MyoIIA knockdown resulted in dispersal of the Golgi ribbon into smaller, discrete Golgi stacks and en face elements characteristic of *trans*-Golgi/TGN, surrounded by large numbers of small uncoated vesicles (Figure 9A; the arrow points to vesicles resembling ‘beads-on-a-string’ while the arrowhead indicates membrane-associated vesicles). Subsequent detailed analysis in 3-dimensions by electron tomography showed pronounced disruption of normal Golgi organization resulting in a mix of pleiomorphic Golgi elements accompanied by numerous uncoated vesicles (Figure 9B, Fig 9B tomo.mov, Fig 9B model.mov). The ‘vesicles’ often appeared to be linked to Golgi membranes by a ‘stalk’ that could well be membrane continuity arising from arrested vesicle fission (Figure 9, A and B, arrowheads). Likewise, groups of vesicles resembling beads-on-a-string suggested the presence of residual membrane continuities (Figure 9B, arrows). Uncoated budding profiles accounted for ~15% of the vesicle-like structures (Figure 9F, Table 2) that appeared to be arrested at various stages of budding (Figure 9F, arrows, rose-colored structures; see also Fig 9F tomo vesicles.mov). Control experiment confirmed MyoIIA depletion by immunolabelling at the light microscope level (Figure 9, C and E), and by Western blotting analysis (Figure 9E; protein knockdown, 81% depletion at 72 h and 93% at 96 h).

In addition to the numerous small, uncoated vesicles, tubular Golgi extensions were observed (Figure 9B, asterisk) consistent with the previous work of Miserey-Lenkei et al. (2010). These tubular profiles were also uncoated. Interestingly, in the examples shown in Figure 9B, one tubule appeared to be condensing into a string of vesicles, likely, examples of incomplete vesicle fission (arrow). Quantitatively, when vesicles were modeled in a representative region of the tomogram (see Fig 9B model.mov), the typical vesicle diameter was ~40 nm (Table 2). For the 7 Golgi stacks scored, the average number of cisternae per stack was 2.71 ± 0.18 and the average maximal cisternal length was 511 ± 19 nm (Table 3). In contrast to the results obtained following Rab6 knockdown, the length of Golgi cisternae in the MyoIIA-depleted cells was slightly shorter compared to control cells and the number of cisternae per stack was reduced (compare Table 1 and 3). Quantitative data obtained from tomograms of the Golgi region in siMyoIIA-treated cells were supported by thin section electron microscope analysis of approximately 20–30 cells per condition. Most importantly, the presence of apparent protein coats on arrested budding profiles was very rare (Figure 9B, “c”, clathrin-coated example; for quantification, see Table 3). In sum, the MyoIIA depletion phenotype does not replicate the phenotype resulting from knockdown of Rab6. Importantly, these results by comparison strongly indicate that the accumulation of coated vesicles, particularly COPI-vesicles that have been implicated previously in Golgi retrograde trafficking and cisternal maturation (43), are central to the observed cisternal proliferation.

DISCUSSION

The results presented here indicate that Rab6 - the most abundant Golgi-associated Rab protein (2) – is essential to the normal transport and budding and/or consumption of multiple classes of coated vesicles. Moreover, they suggest that coated vesicle trafficking is crucial to the role of Rab6 in Golgi homeostasis. These results are a novel and unexpected outcome; considerable evidence to date has implicated Rab6 in non-coated, Golgi-derived vesicle trafficking (e.g., 10,11,42). The experiments themselves and the electron microscope approach essential to this outcome were prompted by our previous findings that in double knockdown, epistasis experiments, that Rab6 was required for the dispersal of Golgi-derived vesicles to the cytosol (Sun et al., 2007). We reasoned that since Rab6 effectors include a number of motor proteins and/or motor interacting polypeptides, e.g., myosin IIA, KIF5B, KIF1C, KIF20 and subunits of the dynactin complex, that the epistatic suppression observed with Rab6 knockdown of both vesicle dispersal and Golgi fragmentation could be due to a failure to transport Golgi-derived vesicles. If so, Rab6 depletion might well produce vesicle accumulation in the immediate proximity of the Golgi apparatus. Because these vesicles would be Golgi proximal, they would be undetectable at the 200 nm or so resolution of the light microscope. Therefore, we used electron microscopy and, in particular, electron tomography of thick sections with its much higher resolution of ~4 nm as our primary experimental readout. In sum, the net outcome of our electron microscopy has been to reveal that Rab6 knockdown produces a diverse set of Golgi phenotypic changes in which the pronounced increase in cisternal number and continuity is accompanied by the accumulation of two classes of vesicles, both coated and concentrated on the *trans* side of the organelle. We propose that the observed accumulation of coated vesicles is primary to the dilation of the *trans*-Golgi/TGN and the proliferation of Golgi cisternae in response to Rab6 depletion.

We have taken the top down approach of knocking out Rab6 (Rab6a/a') to study the role of Rab6 regulated protein machines in the regulation of Golgi dynamics and homeostasis. This approach has the virtue of revealing what are likely the dominant or most important phenotypic consequences of Rab6 for Golgi organization and dynamics. In our initial studies we found that two different siRNAs directed against Rab6 produced the same morphological phenotype in electron micrographs of chemically fixed, thin-sectioned HeLa cells. In both cases, there appeared to be considerable cisternal proliferation, dilation of several cisternae and some accumulation of coated vesicles and cisternal-associated, coated-swellings that we term Ω figures. As both siRNAs produced the same morphological phenotype, we chose in all subsequent experiments to use the siRab6(Sun) previously described by this laboratory (9). In additional validation of this choice, we had shown previously that the Rab6 phenotype suppression is mimicked by overexpression of GDP-restricted Rab6 and in some cases by the overexpression of a mutant Rab6 effector (9). A final methodological outcome from our initial electron microscopy was the decision to use high pressure freezing as the first step in all subsequent sample preparation for electron microscopy. We found that high pressure freezing followed by freeze substitution gave a much better preservation of Golgi structure in Rab6-depleted cells. Under these conditions, cisternal dilation was clearly restricted to the *trans*-Golgi/TGN, the site of coated vesicle accumulation.

To the best of our knowledge, our observations provide the first example in which depletion of an Golgi-associated regulatory molecule resulted in significantly increased Golgi organization, increased cisternal stacking and lateral continuity. In striking contrast, we found that knockdown of a single Rab6 effector, MyoIIA (11), resulted in the accumulation of small, uncoated structures that often remained linked to Golgi membranes but was not accompanied by a concomitant accumulation of multiple classes of coated vesicles or Ω figures as observed for Rab6. In siMyoIIA-treated cells, the general architecture of the Golgi ribbon was disrupted and cisternae within individual Golgi stacks were slightly shorter and

less numerous than in control cells. At the electron microscope level, we did observe evidence for MyoIIA regulated Golgi tubule extension as reported by others (11). Rab6 has also been reported to regulate Golgi tubule extension in response to hypotonic shock (44). As MyoIIA is a known motor protein in Golgi to plasma membrane trafficking (11,42), the failure to observe any increase in Golgi cisternal number with MyoIIA knockdown strongly indicates that inhibition of Golgi to plasma membrane trafficking per se is not tightly coupled to cisternal homeostasis. Our experiments indicate that Rab6-dependent recruitment of a cisternal adherence factor, likely a golgin, is of limited structural consequence to the overall organization of the Golgi apparatus. Although the disruption or depletion of individual golgins can lead to fragmentation of the Golgi ribbon (for review, see 45), we found that Rab6 depletion did not fragment the Golgi ribbon rather the Golgi ribbon was, if anything, more continuous. We did observe some de-adherence of TGN from *trans*-Golgi cisternae and correspondingly *trans*-Golgi cisternae from medial cisternae. Together these observations suggest that a limited set of Rab6 effecters are most important to establishing the morphological organization of the mammalian Golgi apparatus. A major goal of our current research is defining what that crucial subset might be.

The work presented in this paper provides an explanation for the apparent dominant role of Rab6 in Golgi organization that is entirely consistent with our previous double knockdown experiments (9). In epistatic knockdown experiments, Rab6 loss-of-function suppressed Golgi fragmentation following knockdown of either the multimeric COG retrograde tether complex or the putative Golgi retrograde tether proteins ZW10 or RINT1 (for review, see 46). Importantly, co-depletion of Rab6 together with COG suppressed the cytoplasmic accumulation of Golgi-derived vesicles (9), suggestive that Rab6 regulates a key early step in either vesicle formation or transport. Based on the present, we suggest that a major effect of Rab6 is at the level of coated vesicle formation/transport. Whether this is the crucial function of Rab6 in Golgi organization remains an open question. An inhibition of coated vesicle transport, especially that of COPI-coated vesicles, presumed intra-Golgi retrograde carriers, could well have feedback/knock-on effects through delayed recycling on coated vesicle formation and cargo transport through the Golgi apparatus. A primary defect in transport could then have secondary consequences on cisternal progress/maturation and the proliferation of Golgi cisternae. Considering the number of motor proteins known to be Rab6 effectors, we favor the interpretation that the failure to recruit a motor(s) may produce a primary defect in coated vesicle transport that then produces the potential secondary consequences cited previously. In addition, Rab6 may have a hitherto unsuspected role in autophagy and/or non-conventional secretion. We observed the accumulation of multivesicular/autophagic compartments in Rab6 knockdown cells. Whether this is a direct Golgi-associated consequence of Rab6-depletion, or mediated via a second Rab, e.g., Rab33b, a functionally overlapping Golgi Rab (47) known also to be involved in autophagy (48,49) is unknown.

We found that the Rab6-depleted, Golgi apparatus still supported secretory cargo transport, albeit at a slowed rate, a result consistent with the previous evidence of Grigoriev et al (42) and Miserey-Lenkei et al. (11) that Rab6 - facilitated VSV-G transport from the Golgi to plasma membrane. Rab6 has long been known to have diverse effects on Golgi transport kinetics and organization. Depletion of Rab6 is known to affect both anterograde and retrograde Golgi trafficking (11,12,42). Furthermore, Rab6 has been implicated in the regulation of endosome to TGN trafficking (50,51). Overexpression of GTP-restricted Rab6 causes the redistribution of Golgi proteins to the ER (44,52) while, on the other hand, overexpression of GDP-restricted Rab6 delays secretory cargo transport from the TGN to the plasma membrane and inhibits Golgi to ER retrograde trafficking of Golgi enzymes (10,53). Here we found using quantitative fluorescence microscopy that transport of the model cargo protein, VSV-G protein, from the ER to Golgi was unaffected by Rab6-

depletion while transport of VSV-G protein from the Golgi apparatus to the plasma membrane was substantially inhibited. Likely, this inhibition occurs at the *trans*-Golgi/TGN as that is the site of cisternal dilation and coated vesicle accumulation.

We suggest that the two morphological classes of coated vesicles/Ω figures that accumulated in response to Rab6 depletion correspond to clathrin-and COPI-coated structures. This reasoning is based upon the morphology of the coats in electron tomograms where the coat can be observed in different planes and orientation and on the size difference between the two vesicle classes. The one coat appeared to be spikey and the other smooth. The spikey coat was associated with vesicles/Ω structures with an average diameter of ~75 nm while the smooth coat was associated with vesicles/Ω figures of an average diameter of ~45 nm. These properties are consistent with the larger structures being clathrin coated and the smaller COPI coated. Other possible approaches to identifying the coats are immunolabeling and biochemistry/cell fractionation. Biochemically, our previous report that the lysosomal membrane protein LAMP2 is shifted to a higher molecular weight, i.e., further processed, in Rab6 knockdown cells (9) is consistent with the delayed transport implicit in the accumulation of putative clathrin-coated vesicles, known carriers in Golgi to endosome/lysosome cargo transport. Our light microscope immunolabeling experiments with antibody directed against COPI indicate an increase in the level of Golgi associated COPI coat (Storrie, unpublished observations). Our initial efforts at a high-resolution immunogold labeling approach failed to give sufficient labeling to permit any conclusions to be drawn (Micaroni and Marsh, unpublished observations). To date, no direct effector link has been made between Rab6 and COPI or clathrin. However, the linkage to vesicles may well not be to the coat but rather to a motor protein. Several motor proteins are known Rab6 effectors. Whether specific effects due to Rab6a or Rab6a' are evident in our data set remains for now an open question. In our experiments, we have used proven siRNAs directed against both Rab6 isoforms (9,12) and hence the total level of Rab6 protein is knocked down 80 to >95%. The maximal level of total Rab6 protein reduction expected for the knockdown of the individual Rab6a or Rab6a' isoforms is approximately 50%.

In conclusion, we present evidence from the unbiased and high-resolution approach of electron microscopy and electron tomography that Rab6 regulates, be it directly or indirectly, the *trans*-Golgi proximal accumulation of two morphological classes of coated vesicles. The morphological properties of these vesicles are suggestive that one class corresponds to clathrin-coated vesicles and the other to COPI-coated vesicles. Based on the site of vesicle accumulation, cisternal dilation and the kinetics of cargo transport from the ER to the plasma membrane, we suggest that Golgi function in transport is preferentially inhibited at the *trans*-Golgi/TGN. The observed proliferation of Golgi cisternae in Rab6-depleted HeLa cells may then be a secondary consequence of slowed Golgi export and/or inhibited intra-Golgi retrograde trafficking mediated by COPI-coated vesicles. Such an outcome is consistent with a cisternal maturation/progression model of Golgi function in secretion and the accumulated putative COPI vesicles are likely intermediates in cisternal maturation. These results are the first evidence for a Rab6-dependent coated vesicle transport at the *trans*-Golgi and the first example of concomitant cisternal proliferation and increased Golgi stack organization under such conditions.

MATERIALS AND METHODS

Cell Culture

Wild-type HeLa cells were grown in DMEM supplemented with 10% fetal bovine serum (FBS) in a humidified incubator at 37°C and 5% CO_2. HeLa cells stably expressing GalNAcT2-GFP (N-acetylgalactosaminyltransferase-2 fused to the green fluorescent protein

(GFP)) were maintained in culture in the presence of G-418 (54). All cell culture media, sera and associated reagents were obtained either from Invitrogen or the Sigma Chemical Co.

RNA Interference (RNAi) and Nocodazole Treatment

siRab6(Sun) (starting at nucleotide position 554 within the coding sequence of Rab6) used to deplete endogenous Rab6 protein levels in HeLa cells in most experiments was manufactured by Dharmacon RNA Technologies (Lafayette, CO, USA) and was directed against a 3' portion of Rab6 mRNA that is common to both the Rab6a and Rab6a' isoforms generated by alternative splicing of the Rab6A gene (9,55). Consequently, we use the term 'Rab6' in this paper to collectively refer to both splice variants. Rab6a and Rab6a' differ by only three amino acids, share the same GTP binding properties, localize to the Golgi and are at least partially functionally redundant (12,55). Under the conditions used in our experiments, we achieved a 75–95% depletion of Rab6 by RNAi knockdown over a 72–96 h period (Figures 1C, 2C and 3G) (9) accompanied by a high level of phenotypic penetrance (95–96%, data not shown), consistent with previous results (9). In some experiments, an alternate siRNA directed against the 5' third of Rab6 starting at nucleotide position 78 (siRab6(Young), 12) was used. For MyoIIA knockdown, the following siRNA: AGGAGUUUCGGCAGAGAGAUAUU, synthesized by Dharmacon was used (11). siRNA transfections using Oligofectamine (Invitrogen) were carried out in the absence of FBS using previously described protocols with only minor modifications (9,12). In brief, 70,000 cells in a 35 mm dish underwent two successive cycles of siRNA transfection for maximal knockdown; the second cycle started 24 h after the initial incubation (Sun et al., 2007). Protein depletion times are referenced to the first transfection cycle. The scrambled siControl RNA has been described previously (9).

siControl and siRab6 HeLa cell cultures were exposed to nocodazole as previously described (54,56).

Antibodies

Rabbit antibodies directed against Rab6, β-actin and TGN46 were purchased commercially and used as described elsewhere (9,44,57). Rabbit antibodies to β-COP were purchased from Santa Cruz Biotechnology, Inc. (Santa Cruz, CA, USA) and those against the C-terminal peptide of human MyoIIA were purchased from Covance, Inc (Princeton, NJ, USA). Monoclonal antibodies against gpp130, an ectoepitope of ts045-VSV-G protein, and β-COP were gifts from Adam Linstedt (Dept. of Biology, Carnegie Mellon University, Pittsburgh, PA, USA), Harvey Lodish (Dept. of Biology, Massachusetts Institute of Technology, Cambridge, MA, USA), and James E. Rothman (Department of Cell Biology, Yale University), respectively.

Chemical Fixation for Thin Section Electron Microscopy

RNAi treated cells were grown in 35 mm tissue culture dishes and fixed in situ with 0.05% malachite green, 2.5% glutaraldehyde in 0.1 M cacodylate buffer as described (58). Cells were then stained with osmium tetroxide followed by sequentially by tannic acid and uranyl acetate. Cells were then scraped off the tissue culture dish, dehydrated, and plastic embedded. Thin sections were cut at 40 or 50 nm thickness with a Leica UltraCut 7 microtome and examined at an accelerating voltage of 80 KeV with a Tecnai F20 intermediata voltage electron microscope (FEI Co.). Images were collected with a 4K FEI Eagle CCD camera.

Western Blot Analysis

HeLa cells were lysed in 2% SDS, followed by standard SDS-PAGE (12% acrylamide) and Western blotting essentially as previously described (9,59). Western blots were quantified using a LI-COR Odyssey system (LI-Cor Biosciences, Lincoln, NE).

VSV-G Transfection and Chase

After 80 h incubation with either scrambled (control) or siRNA against Rab6, wild type HeLa cells were transfected with plasmids encoding tsO45 mutant of VSV-G-GFP protein and incubated overnight at 39.5 C, non-permissive conditions for the transport of VSV-G protein from the ER to Golgi apparatus. Cells were then shifted to 32°C, permissive conditions for tsO45 G transport, and incubated for various chase in the presence of cycloheximide to prevent further protein synthesis. Cells were then fixed with paraformaldehyde and cell surface stained for VSV-G protein and subsequently intracellularly stained for Rab6 expression level. Under these conditions, the total siRNA treatment time was 4 d. Plasmid expression was deliberately chosen to give a low expression level for VSV-G protein.

Fluorescence Microscopy and Image Processing

To characterize protein distributions by immunofluorescence at the light microscope level, fixed cells were visualized either using a BD CARVII spinning disk confocal microscopy accessory mounted on a Zeiss 200M inverted microscope controlled by *iVision-Mac* software (BioVision Technologies, Exton, PA, USA) to give confocal image stacks or directly with the Zeiss 200M inverted microscope to give wide field micrographs. Images were collected with a 63x/1.40 numerical aperture objective and subsequently processed using *iVision-Mac* software.

To assess qualitatively the effect of Rab6 knockdown on Golgi phenotype prior to correlative imaging at the electron microscopy level, GalNAcT2-GFP expressing HeLa cells treated with siRab6 (together with control HeLa cells transfected with scrambled/nonsense siRNA duplexes) cultured on gold EM finder grids (Electron Microscopy Sciences, Hatfield, PA, USA) were imaged at 37 °C using a heated stage mounted on a Zeiss LSM 510 microscope. Image stacks were taken as rapidly as possible at a spacing of 1 μm using a 63x/1.40 numerical aperture objective and a zoom factor of 0.7 or 1.0 to accommodate a large field of view. During image acquisition, HeLa cells were maintained in PBS supplemented with 2% FBS. Resulting image sets were compressed into maximum intensity projections using *ImageJ* software.

To quantify the effects of nocodazole on the distribution of the Golgi marker, GalNAcT2-GFP, maximum intensity projections of full cell depth HeLa cell confocal image stacks were analyzed using *iVision-Mac* software. For the assessment of nocodazole scattered peripheral Golgi elements, a size criteria of 0.078 to 2.70 μm^2 (10–350 pixels, 0.0879 μm pixel size) was assigned and the number of GalNAcT2-GFP structures falling into that size was computer scored. For the assessment of BFA-induced Golgi dispersal to the ER, image segmentation of maximum intensity projections was used to determine total cell GalNAcT2-GFP fluorescence and juxtanuclear Golgi fluorescence. Golgi fluorescence was subtracted from total cell fluorescence to give ER associated Golgi fluorescence.

To quantify total VSV-G protein distribution between a juxtanuclear Golgi accumulation and the ER, VSV-G-GFP expressing cells imaged with wide field optics and then juxtanuclear VSV-G-GFP and total cellular G protein were determined by outlining the appropriate areas manually and the mean pixel intensity in the juxtanuclear Golgi area and the total was determined with *iVision-Mac* software. To quantify VSV-G cell surface

labeling, VSV-G plasmid transfected cells were surface labeled for extracellular VSV-G protein epitope and imaged. Stained cells were outlined manually and the mean pixel intensity per cell determined with *iVision-Mac* software. All pixel intensities were corrected for background fluorescence as determined by outlining non-cellular areas within the images.

High-Pressure Freezing, Freeze-Substitution and Microtomy

Following live cell imaging at 37 °C as described above to establish phenotype penetrance, both Rab6-depleted and control HeLa cells grown on gold finder grids were high-pressure frozen essentially as described previously (15,22,60). Solutions and metal specimen holders (Swiss Precision Inc., Millbrae, CA, USA) for high-pressure freezing were pre-warmed to 37 °C, and all manipulations were performed on an inverted heating block warmed to 37 °C under a dissecting microscope (Olympus, Australia). Following high-pressure freezing using either a BAL-TEC HPM010 or Leica EM PACT2 high-pressure freezing units (Leica Microsystems), cells frozen on grids were stored in liquid nitrogen. Specimens were freeze-substituted using a Leica AFS unit (Leica Microsystems) and then plastic-embedded essentially as described previously (15,22,60).

Electron Microscopy and Cellular Electron Tomography

The procedures used to prepare mammalian cells for electron microscopy/electron tomography imaging and subsequent 3D reconstruction using a dual-axis tomography approach have been described elsewhere in detail (15,22,60–62). Briefly, both thin (40–60 nm) and thick (300–400 nm) sections cut with a Leica UltraCut-UCT microtome were collected onto Formvar-coated copper slot grids and post-stained with aqueous uranyl acetate and Reynold's lead citrate (Electron Microscopy Sciences, Hatfield, PA, USA) to enhance contrast/visualization. Thin sections were surveyed using a JEOL 1200 electron microscope (JEOL Australasia Pty Ltd.) operated at 80–120 KeV to assess the quality of ultrastructural preservation, collect sets of 2D images depicting representative Golgi regions in both Rab6-depleted and control cells, and for the identification of cells for subsequent tomographic imaging/reconstruction based on correlated light microscope images of the same grids prior to freezing. For electron tomography, thick sections were imaged with a Tecnai F30 intermediate-voltage electron microscope operated at 300 KeV (FEI Co.) using motorized tilt-rotate specimen holders (Models 650 and CT3500TR; GATAN Inc., Pleasanton, CA, USA). Tilt series datasets were collected at 20000 or 23000x magnification either by single panel CCD (charge-coupled device) imaging or by image montaging (2 × 2 panels) using automated data acquisition and image alignment routines as the grids housing the sections were serially tilted over a range of ~120° (±60°) and about two orthogonal axes using the microscope control program *SerialEM* (63,64). Tomograms computed from aligned 2D views for each single-axis dataset were computationally registered and combined in 3D space to produce a dual-axis tomogram for quantitative analysis that encompassed a cellular area measuring ~4.3 × 4.3 μm in X and Y, with a final pixel size of 2.144 nm, siControl and siRab6 samples and for siMyoIIA samples the cellular area was ~4.75 × 4.75 μm in XY, with a final pixel size of 1.26 nm.

All of the above procedures - along with subsequent protocols for image segmentation, surface mesh computation/generation, 3-dimensional visualization and quantitative analysis - were performed using the *IMOD* software package maintained and distributed by the Boulder Laboratory for 3D Electron Microscopy of Cells at the University of Colorado (Boulder, CO, USA)(65), essentially as described previously (15,22). Quantification of 2D images acquired from thin sections cut from high-pressure frozen cells was carried out for 11–14 cells for Rab6-depleted *versus* controls. High-resolution 3D reconstructions of the Golgi region generated for 4–5 cells for Rab6-depleted HeLa cells (likewise for controls)

were qualitatively evaluated by comparison to one another, and to 2D images of thin sections as well as correlated light microscope data for Golgi phenotypes. Tomograms assessed as 'representative' for siRab6-treated versus control cells were subsequently segmented in 3D for detailed quantitative analysis and comparative 3D visualization of Golgi structure/organization. The color-coding for different segmented membranes and vesicles is listed for relevant Figures in the legend. siMyoIIA samples were handled similarly. Supplementary multimedia video files of the 3D datasets were made as QuickTime® movies from file sequences generated directly from the *3dmod* viewer window in *IMOD*. Movies of the 3D reconstructions with/without model contours overlaid as colored line segments were generated as the tomogram image slice was advanced in Z; movies of the surface-rendered models generated from cellular tomograms by meshing segmentation contours on adjacent image slices in Z display 3D models of the Golgi as they are incrementally rotated in X or Y to allow unobstructed views of the structures.

Supplementary Material

Refer to Web version on PubMed Central for supplementary material.

Acknowledgments

We greatly appreciate the provision of siRNA sequences directed against MyoIIA prior to publication by Dr. Bruno Goud, Institut Curie, Paris. We also appreciate his repeated comments on the work and on the manuscript. We gratefully acknowledge the comments of Dr. Kimberly Forsten Williams, Virginia Tech, Blacksburg, VA on the final draft of this paper. We gratefully acknowledge Matthias Floetenmeyer and Darren Paul for their assistance in facilitating access to the EM and LM core facilities, respectively, housed within the Institute for Molecular Bioscience. This work was supported by National Science Foundation (NSF, USA; MCB-0549001) and National Institutes of Health (NSF, USA; 1R01 GM-092206) grants and National Institute of Standards and Technology (NIST, USA) subaward to BS and a National Health and Medical Research Council (NHMRC, Australia; 569535) grant to BJM and BS. The 'Advanced Cryo-Electron Microscopy Laboratory' is a major node of the Australian Microscopy and Microanalysis Research Facility (AMMRF) funded by the Australian Federal government. The 'ACRF Cancer Biology Imaging Facility' is funded by the Australian Cancer Research Foundation (ACRF). Both facilities are supported by the Queensland State government's 'Smart State Strategy' initiative.

Abbreviations

COPI	coat protein I
COPII	coat protein II
ER	endoplasmic reticulum
ERGIC	ER-Golgi intermediate compartment
FBS	fetal bovine serum
KeV	kilo electron volts
GalNAcT2-GFP	N-acetylgalactosaminyltransferase-2 (GalNAcT2) fused to the green fluorescent protein (GFP)
MyoIIA	myosin IIA
RNAi	RNA interference
siRNA	small interfering ribonucleic acid
TGN	*trans*-Golgi network
VSV-G	vesicular stomatitis virus membrane glycoprotein

References

1. Hutaqalung AH, Novick PJ. Role of Rab GTPases in membrane traffic and cell physiology. Physiol Rev. 2011; 91:119–149. [PubMed: 21248164]
2. Gilchrist A, Au CE, Hiding J, Bell AW, Fernandez-Rodriguez J, Lesimple S, Nagaya H, Roy L, Goslins SJ, Hallett M, Paiement J, Kearney RE, Nilsson T, Bergeron JJ. Quantitative proteomics analysis of the secretory pathway. Cell. 2006; 127:1265–1281. [PubMed: 17174899]
3. Darchen F, Goud B. Multiple aspects of Rab protein action in the secretory pathway: focus on Rab3 and Rab6. Biochimie. 2000; 82:375–384. [PubMed: 10865125]
4. Opham FJ, Echard A, Cross HJ, wan den Hurk JA, wan de Vorstenbosch RA, Ginsel LA, Goud B, Fransen JA. The small GTPase Rab6B, a novel Rab6 subfamily member, is cell-type specifically expressed and localized to the Golgi apparatus. J Cell Sci. 2000; 113:2725–2735. [PubMed: 10893188]
5. Simpson JC, Wellenreuther R, Poustka A, Pepperkok R, Wiemannn S. Systemic subcellular localization of novel proteins identified by large-scale cDNA ssequencing. EMBO Rep. 2000; 1:287–292. [PubMed: 11256614]
6. Shan J, Yuan L, Budman DR, Xu HP. WTH3, a new member of the Rab6 gene family, and multidrug resisteance. Biochim Biophys Acta. 2002; 1589:112–123. [PubMed: 12007787]
7. Young J, Ménétrey J, Goud B. RAB6C is a retrogene that encodes a centrosomal protein involved in cell cycle progression. J Mol Biol. 2010; 397:69–88. [PubMed: 20064528]
8. Fernandes H, Franklin E, Recacha R, Houdussa A, Goud B, Khan AR. Structural aspcects of Rab6-effetor complexes. Biochem Soc Trans. 2009; 37:1037–1041. [PubMed: 19754447]
9. Sun Y, Shestakova A, Hunt L, Sehgal S, Lupashin V, Storrie B. Rab6 regulates both ZW10/RINT-1 and conserved oligomeric Golgi complex-dependent Golgi trafficking and homeostasis. Mol Biol Cell. 2007; 18:4129–4142. [PubMed: 17699596]
10. Girod A, Storrie B, Simpson JC, Johannes L, Goud B, Roberts LM, Lord JM, Nilsson T, Pepperkok R. Evidence for a COP-I-independent transport route from the Golgi complex to the endoplasmic reticulum. Nat Cell Biol. 1999; 1:423–430. [PubMed: 10559986]
11. Miserey-Lenkei S, Chalancon G, Bardin S, Formstecher E, Goud B, Echard A. Rab and actomyosin-dependent fission of transport vesicles at the Golgi complex. Nat Cell Biol. 2010; 12:645–654. [PubMed: 20562865]
12. Young J, Stauber T, del Nery E, Vernos I, Pepperkok R, Nilsson T. Regulation of microtubule-dependent recycling at the trans-golgi network by Rab6A and Rab6A′. Mol Biol Cell. 2005; 16:162–177. [PubMed: 15483056]
13. Mallabiabarrena A, Malhotra V. Vesicle biogenesis: the coat connection. Cell. 1995; 83:667–669. [PubMed: 8521481]
14. Ladinsky MS, Mastronarde DN, McIntosh JR, Howell KE, Staehelin LA. Golgi structure in three dimensions: functional insights from the normal rat kidney cell. J Cell Biol. 1999; 144:1135–1149. [PubMed: 10087259]
15. Marsh BJ, Mastronarde DN, Buttle KF, Howell KE, McIntosh JR. Organellar relationships in the Golgi region of the pancreatic beta cell line, HIT-T15, visualized by high resolution electron tomography. Proc Natl Acad Sci USA. 2001; 98:2399–2406. [PubMed: 11226251]
16. Marsh BJ, Mastronarde DN, McIntosh JR, Howell KE. Structural evidence for multiple transport mechanisms through the Golgi in the pancreatic beta-cell line, HIT-T15. Biochem Soc Trans. 2001; 29:461–467. [PubMed: 11498009]
17. Ladinsky MS, Wu CC, McIntosh S, McIntosh JR, Howell KE. Structure of the Golgi and distribution of reporter molecules at 20 degrees C reveals the complexity of the exit compartments. Mol Biol Cell. 2002; 13:2810–2825. [PubMed: 12181348]
18. Matlin KS, Simons K. Reduced temperature prevents transfer of a membrane glycoprotein to the cell surface but does not prevent terminal glycosylation. Cell. 1983; 34:233–243. [PubMed: 6883510]
19. Matlin KS, Simons K. Sorting of an apical plasma membrane glycoprotein occurs before it reaches the cell surface in cultured epithelial cells. J Cell Biol. 1984; 99:2131–2139. [PubMed: 6501415]

20. Saraste J, Palade GE, Farquhar MG. Temperature-sensitive steps in the transport of secretory proteins through the Golgi complex in exocrine pancreatic cells. Proc Natl Acad Sci USA. 1986; 83:6425–6459. [PubMed: 3462704]
21. Grifftihs G, Fuller SD, Back R, Hollinshead M, Pfeiffer S, Simons K. The dynamic nature of the Golgi complex. J Cell Biol. 1989; 108:277–297. [PubMed: 2537312]
22. Marsh BJ, Volkmann N, McIntosh JR, Howell KE. Direct continuities between cisternae at different levels of the Golgi complex in glucose-stimulated mouse islet beta cells. Proc Natl Acad Sci USA. 2004; 101:5565–5570. [PubMed: 15064406]
23. Donohoe BS, Kang BH, Staehelin LA. Identification and characterization of COPIa- and COPIb-type vesicle classes associated with plant and algal Golgi. Proc Natl Acad Sci U S A. 2007; 104:163–168. [PubMed: 17185411]
24. Marsh BJ, Howell KE. The mammalian Golgi -complex debates. Nat Rev Mol Cell Biol. 2002; 3:789–795. [PubMed: 12360195]
25. Donohoe BS, Mogelsvang S, Staehelin LA. Electron tomography of ER, Golgi and related membrane systems. Methods (San Diego, Calif). 2006; 39:154–162.
25. Koster AJ, Klumperman J. Electron microscopy in cell biology: integrating structure and function. Nat Rev Mol Cell Biol. 2003; (Suppl):SS6–10. [PubMed: 14587520]
26. Mogelsvang S, Marsh BJ, Ladinsky MS, Howell KE. Predicting function from structure: 3D structure studies of the mammalian Golgi complex. Traffic. 2004; 5:338–345. [PubMed: 15086783]
27. Trucco A, Polishchuk RS, Martella O, Di Pentima A, Fusella A, Di Giandomenico D, San Pietro E, Beznoussenko GV, Polishchuk EV, Baldassarre M, et al. Secretory traffic triggers the formation of tubular continuities across Golgi sub-compartments. Nat Cell Biol. 2004; 6:1071–1081. [PubMed: 15502824]
28. Marsh BJ. Lessons from tomographic studies of the mammalian Golgi. Biochim Biophys, Acta. 2005; 1744:273–292. [PubMed: 15896857]
29. De Matteis MA, Luini A. Exiting the Golgi complex. Nat Rev Mol Cell Biol. 2008; 9:273–284. [PubMed: 18354421]
30. Emr S, Glick BS, Linstedt AD, Lippincott-Schwartz J, Luini A, Malhotra V, Marsh BJ, Nakano A, Pfeffer SR, Rabouille C, et al. Journeys through the Golgi - taking stock in a new era. J Cell Biol. 2009; 187:449–453. [PubMed: 19948493]
31. Farquhar MG, Palade GE. The Golgi apparatus (complex)-(1954–1981)-from artifact to center stage. J Cell Biol. 1981; 91:77s–103s. [PubMed: 7033246]
32. Farquhar MG, Palade GE. The Golgi apparatus: 100 years of progress and controversy. Trends Cell Biol. 1998; 8:2–10. [PubMed: 9695800]
33. Rambourg A, Clermont Y. Three-dimensional electron microscopy: structure of the Golgi apparatus. Eur J Cell Biol. 1990; 51:189–200. [PubMed: 2190832]
34. Novikoff AB. The endoplasmic reticulum: a cytochemist's view (a review). Proc Natl Acad Sci USA. 1976; 73:2781–2787. [PubMed: 183210]
35. Quatacker JR. Different aspects of membrane differentiation at the inner side (GERL) of the Golgi apparatus in rabbit luteal cells. Histochem J. 1979; 11:399–416. [PubMed: 500396]
36. Hermo L, Green H, Clermont Y. Golgi apparatus of epithelial principal cells of the epididymal initial segment of the rat: structure, relationship with endoplasmic reticulum, and role in the fomration of secretory vesicles. Anat Rec. 1991; 229:159–176. [PubMed: 1849381]
37. Orci L, Perrelet A, Rothman JE. Vesicles on strings: morphological evidence for processive transport within the Golgi stack. Proc Natl Acad Sci USA. 1998; 95:2279–2283. [PubMed: 9482876]
38. Efimov A, Kharitonov A, Efimova N, Loncarek J, Miller PM, Andreyeva N, Gleeson P, Galjart N, Maia AR, McLeod IX, et al. Asymmetric CLASP-dependent nucleation of noncentrosomal microtubules at the trans-Golgi network. Dev Cell. 2007; 12:917–930. [PubMed: 17543864]
39. Duran JM, Anjard C, Stefan C, Loomis WF, Malhotra V. Unconventional secretion of Acb1 is mediaed by autophagosomes. J Cell Biol. 2010; 189:527–536. [PubMed: 20440001]

40. Perez-Victoria FJ, Schindler C, Magadan JG, Mardones GA, Delevoye C, Romano M, Raposo G, Bonifacino JS. Ang2/fat-free is a conserved subunit of the Golgi-associated retrograde protein (GARP) complex. Mol Biol Cell. 2010; 21:3386–3395. [PubMed: 20685960]
41. Reggiori F, Klionsky DJ. Autophagy in the eukaryotic cell. Eukaryot Cell. 2003; 1:11–21. [PubMed: 12455967]
42. Grigoriev I, Splinter D, Keijzer N, Wulf PS, Demmers J, Ohtsuka T, Modesti M, Maly IV, Grosveld F, Hoogenraad CC, et al. Rab6 regulates transport and targeting of exocytotic carriers. Dev Cell. 2007; 13:305–314. [PubMed: 17681140]
43. Glick BS, Nakano A. Membrane traffic within the Golgi apparatus. Annu Rev Cell Biol Dev Biol. 2009; 25:113–132.
44. Jiang S, Storrie B. Cisternal rab proteins regulate Golgi apparatus redistribution in response to hypotonic stress. Mol Biol Cell. 2005; 16:2586–2596. [PubMed: 15758030]
45. Barr FA, Short B. Golgins in the structure and dynamics of the Golgi apparatus. Curr Opin Cell Biol. 2003; 15:405–413. [PubMed: 12892780]
46. Sztul E, Lupashin V. Role of vesicle tethering factors in the ER-Golgi membrane traffic. FEBS Lett. 2009; 583:3770–3783. [PubMed: 19887069]
47. Starr T, Sun Y, Wilkins N, Storrie B. Rab33b and Rab6 are functionally overlapping regulators of Golgi homeostasis and trafficking. Traffic. 2010; 11:626–636. [PubMed: 20163571]
48. Fukuda M, Itoh T. Direct link between Atg protein and small GTPase Rab: Atg16L functions as a potential Rab33 effector in mammals. Autophagy. 2008; 4:824–826. [PubMed: 18670194]
49. Itoh T, Fujita N, Kanno E, Yamamoto A, Yoshimori T, Fukuda M. Golgi-resident small GTPase Rab33b interacts with Atg16L and modulates autophagosome formation. Mol Biol Cell. 2008; 19:2916–2925. [PubMed: 18448665]
50. Mallard F, Tang BL, Galli T, Tenza D, Saint-Pol A, Yue X, Antony C, Hong W, Goud B, Johannes L. Early/recycling endosomes-to-TGN transport involves two SNARE complexes and a Rab6 isoform. J Cell Biol. 2002; 156:653–664. [PubMed: 11839770]
51. Miserey-Lenkei S, Coudel-Courteille A, Del Nery E, Bardin S, Piel M, Racine V, Sibarita JB, Perez F, Bornens M, Goud B. A role for the Rab6a′ GTPase in the inactivation of the Mad2-spindle checkpoint. EMBO J. 2006; 25:278–289. [PubMed: 16395330]
52. Martinez O, Antony C, Pehau-Arnaudet G, Berger EG, Salamero J, Goud B. GTP-bound forms of rab6 induce the redistribution of Golgi proteins into the endoplasmic reticulum. Proc Natl Acad Sci USA. 1997; 94:1828–1833. [PubMed: 9050864]
53. Martinez O, Schmidt A, Salamero J, Hoflack B, Roa M, Goud B. The small GTP-binding protein rab6 functions in intra-Golgi transport. J Cell Biol. 1994; 127:1575–1589. [PubMed: 7798313]
54. Storrie B, White J, Röttger S, Stelzer EH, Suganuma T, Nilsson T. Recycling of Golgi-resident glycosyltransferases through the ER revieals a novel pahtway and provides an explanation for nocodazole-induced Golgi scattering. J Cell Biol. 1998; 143:1505–1521. [PubMed: 9852147]
55. Echard A, Opdam FJ, de Leeuw HJ, Jollivet F, Savelkoul P, Hendriks W, Voorberg J, Goud B, Fransen JA. Alternative splicing of the human Rab6A gene generates two close but functionally different isoforms. Mol Biol Cell. 2000; 11:3819–3833. [PubMed: 11071909]
56. Yang W, Storrie B. Scattered Golgi elements during microtubule disruption are initially enriched in trans-Golgi proteins. Mol Biol Cell. 1998; 9:191–207. [PubMed: 9437000]
57. Jiang S, Rhee SW, Gleeson PA, Storrie B. Capacity of the Golgi apparatus for cargo transport prior to complete assembly. Mol Biol Cell. 2007; 17:4105–4117. [PubMed: 16837554]
58. Cocchiaro JL, Kumar Y, Fischer ER, Hackstadt T, Valdivia RH. Cytoplasmic lipid droplets are translocated into the lumen of the Chlamydia trachomatis parasitophorous vacuole. Proc Natl Acad Sci USA. 2008; 105:9379–9384. [PubMed: 18591669]
59. Shestakova A, Zolov S, Lupashin V. COG complex-mediated recycling of Golgi glycosyltransferases is essential for normal protein glycosylation. Traffic. 2006; 7:191–204. [PubMed: 16420527]
60. Noske AB, Costin AJ, Morgan GP, Marsh BJ. Expedited approaches to whole cell electron tomography and organelle mark-up in situ in high-pressure frozen pancreatic islets. J Struct Biol. 2008; 161:298–313. [PubMed: 18069000]

61. Marsh BJ. Reconstructing mammalian membrane architecture by large area cellular tomography. Methods Cell Biol. 2007; 79:193–220. [PubMed: 17327158]

62. Mastronarde DN. Dual-axis tomography: an approach with alignment methods that preserve resolution. J Struct Biol. 1997; 120:343–352. [PubMed: 9441937]

63. Mastronarde DN. SerialEM: A program for automated tilt series acquisition on Tecnai microscopes using prediction of specimen position. Microsc Microanat. 2003; 9:1182–1183.

64. Mastronarde DN. Automated electron microscope tomography using robust prediction of specimen movements. J Struct Biol. 2005; 152:36–51. [PubMed: 16182563]

65. Kremer JR, Mastronarde DN, McIntosh JR. Computer visualization of three-dimensional image data using IMOD. J Struct Biol. 1996; 116:71–76. [PubMed: 8742726]

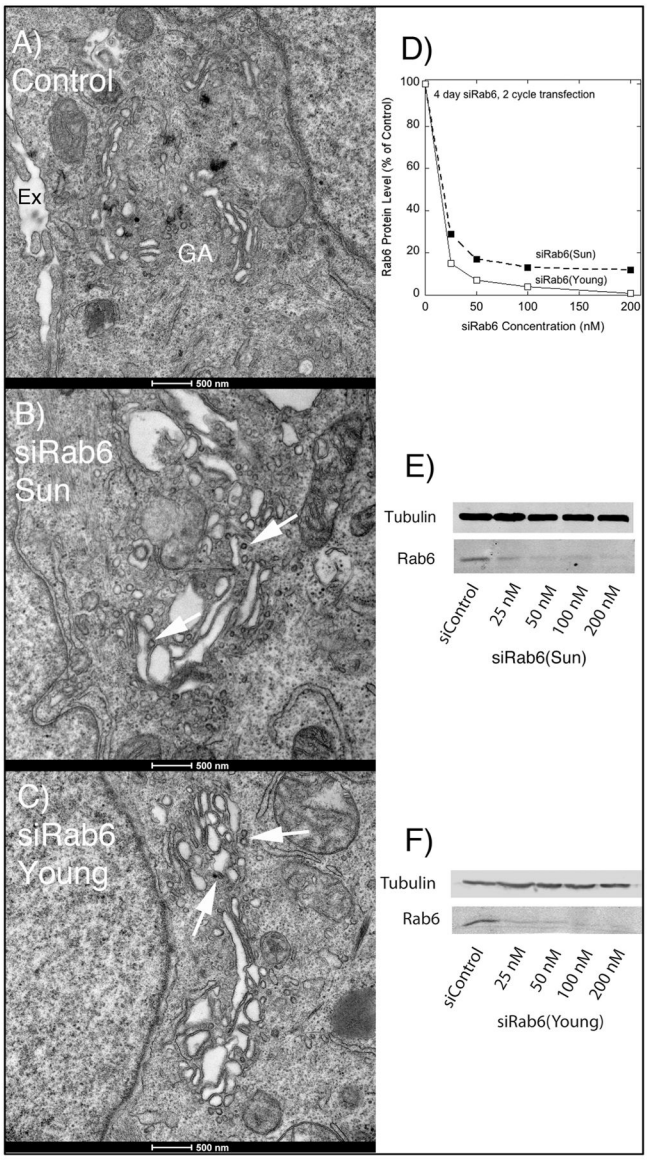

Fig. 1. Treatment of GalNAcT2-GFP HeLa cells with either of two different siRNAs directed against Rab6 results in a similarly expanded Golgi apparatus by electron microscopy

Cells were chemically fixed and then thin sectioned. A: Appearance of the Golgi apparatus (GA) in chemically fixed cells treated with a Control siRNA, extracellular space (Ex). B: Appearance of the Golgi apparatus in chemically fixed cells treated with siRab6(Sun) for 4 d to deplete Rab6 protein levels (see D, E, F). C: Appearance of the Golgi apparatus in chemically fixed cells treated with siRab6(Young) for 4 d to deplete Rab6 protein levels (see D, E, F). Arrows in B and C point to examples of accumulated coated vesicles of various sizes.

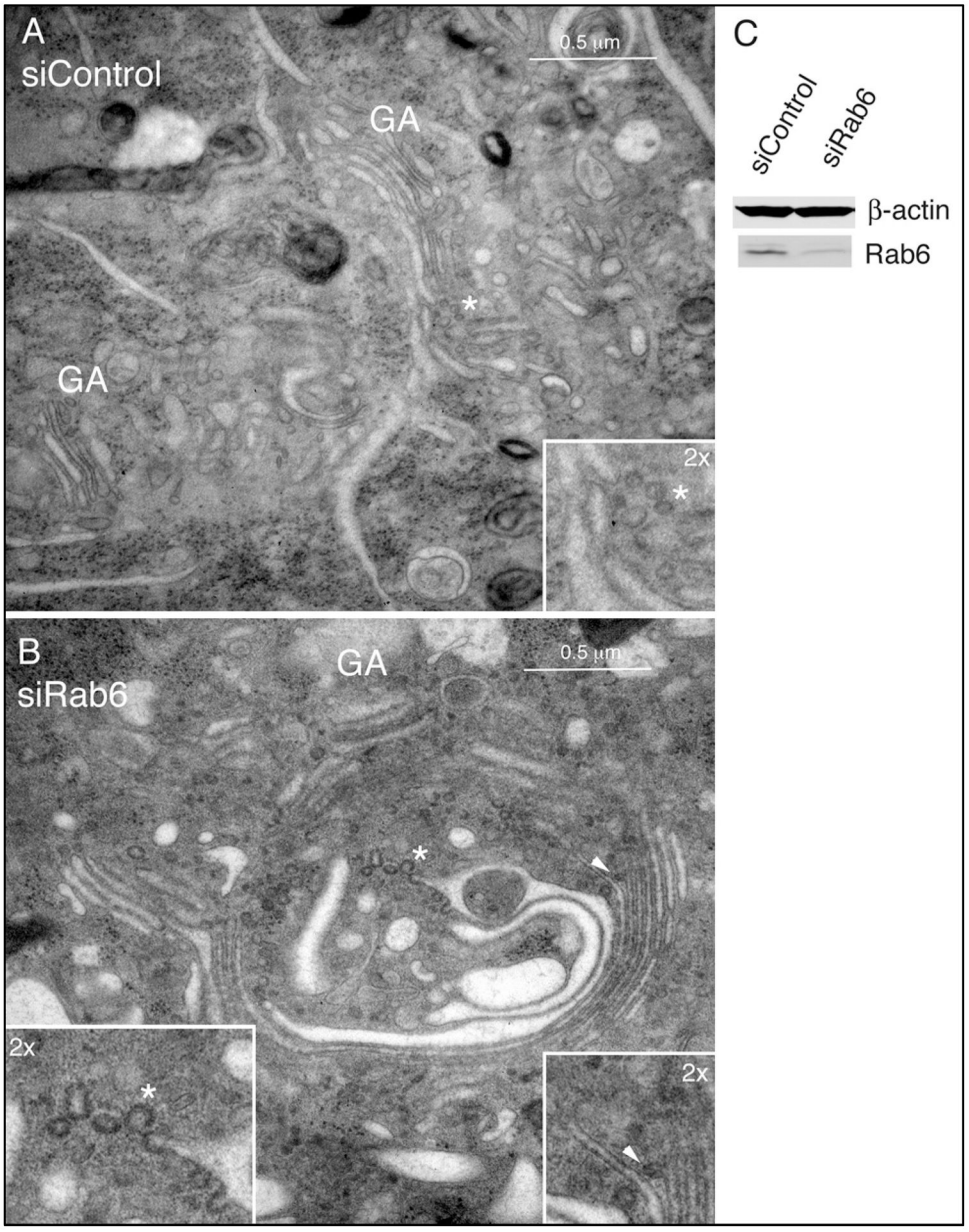

Fig. 2. Rab6-depletion arrests Golgi vesicle release and results in increased cisternal number as well as increased lateral continuity along the length of the Golgi ribbon

HeLa cells stably expressing GalNAcT2-GFP were incubated with siControl (A) or siRNA sequences specific for both the Rab6a and Rab6a' isoforms (B) for 72 h, followed by processing for electron microscopy by high-pressure freezing (A and B) or Western blot analysis (C). GA, Golgi apparatus. Asterisks indicate subregions relatively enriched for arrested vesicle profiles within the larger Golgi region per se, consistent with the lateral rims of cisternae/non-compact regions where vesicular traffic is more prevalent (2x magnification, insets). The asterisk in B highlights an example of clathrin-coated profile as denoted by the spiked, electron-dense coat (2x magnification, inset). The arrowhead in B highlights an example of a putative COPI-coated budding profile attached at the level of medial-cisternae (2x magnification, inset). Bar, 0.5 μm (A and B).

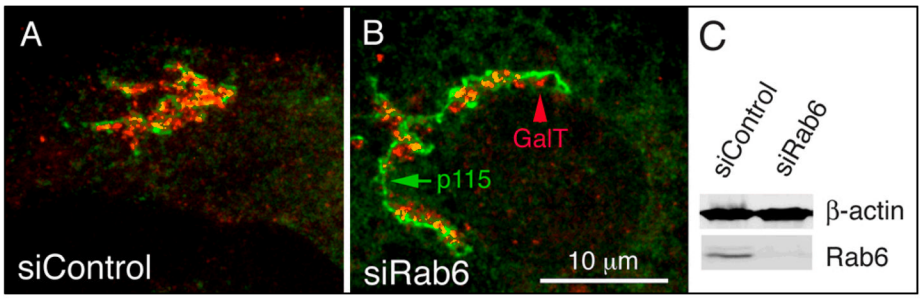

Fig. 3. Golgi stacks in Rab6-depleted cells retain a polarized distribution of resident Golgi proteins along the *cis-trans* axis

Wild-type HeLa cells incubated with either scrambled (siControl, A) or Rab6 siRNA (siRab6, B) for 96 h were fixed for indirect immunofluorescence localization using antibodies specific for p115 and β-galactosyltransferase (GalT). Images shown are maximum intensity projections of confocal image stacks. (C) HeLa cell cultures were processed by Western blot analysis to confirm the efficiency of Rab6 protein knockdown. Bar, 10 μm (A and B).

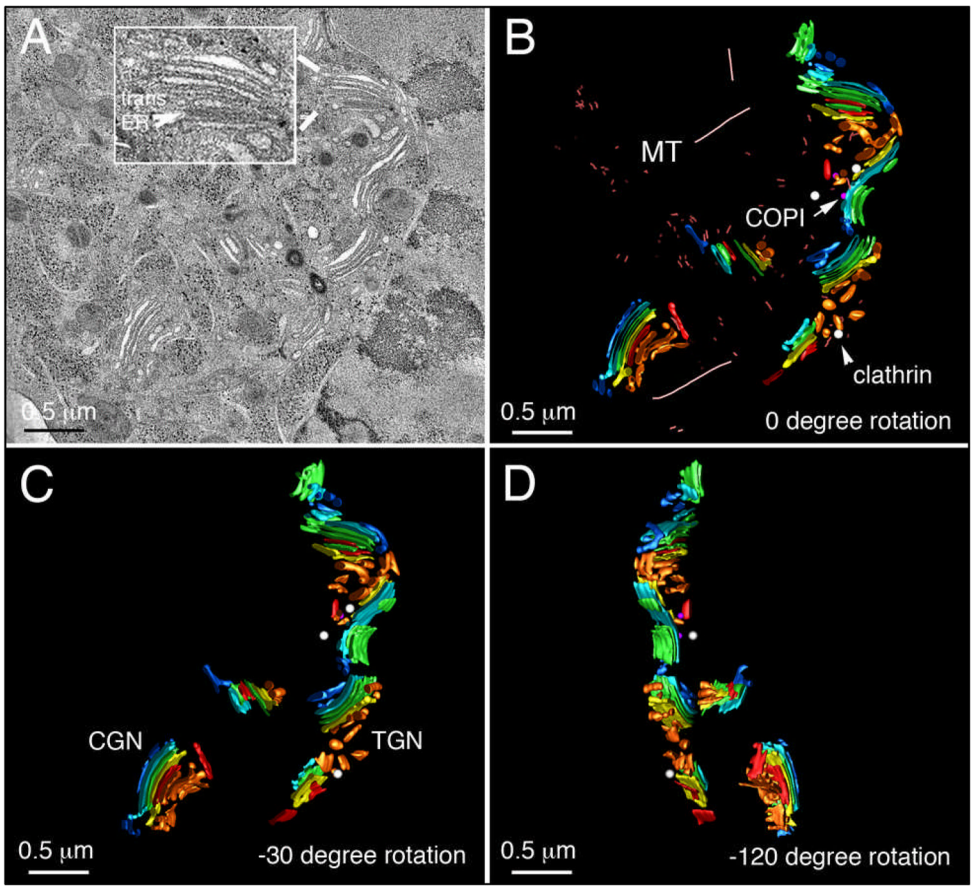

Fig. 4. The Golgi ribbon in control cells is organized as a series of 'compact regions' of stacked cisternae

HeLa cells were treated for 96 h with control siRNA and then high-pressure frozen immediately from 37°C. (A) A representative Golgi ribbon is shown; inset - an example of ER membranes in close physical apposition with *trans*-Golgi cisternae (*trans*-ER, tER). (B) The 3D s model derived from (A) illustrating Golgi spatial organization. (C) Model clockwise rotated −30° about the vertical axis. (D) Model clockwise rotated −120° about the vertical axis. CGN, *cis*-Golgi network; MT, microtubule; TGN, *trans*-Golgi network. Color-coding: *cis*-cisternae/CGN, blue; clathrin-coated vesicles, white; COPI vesicles, purple; ER, red; medial Golgi cisternae, green; *trans*-Golgi, yellow; *trans*-cisternae/TGN, tan. Bar, 0.5 μm.

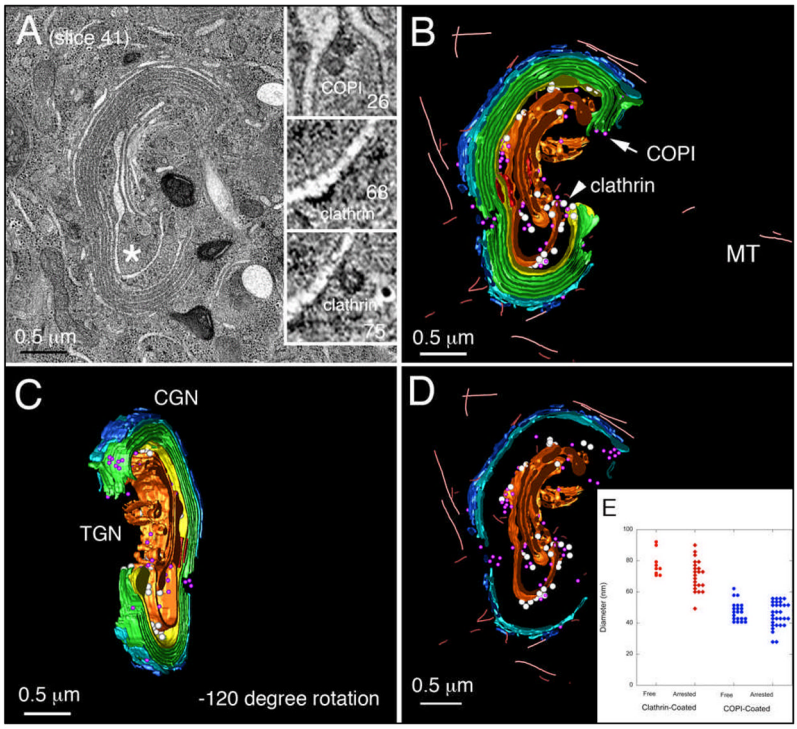

Fig. 5. The Golgi ribbon in Rab6-depleted cells exhibits elongated cisternae/lateral continuity, increased cisternal stacking and extensive arrest of vesicular budding

HeLa cells were incubated with siRab6 for 96 h then high pressure frozen immediately from 37°C. (A) Tomogram; inset, 5.6x view of Z slices from area proximal to asterisk more clearly reveals the spiked, clathrin coat-protein associated with *trans*-Golgi/TGN. (B and C) 3D models of Golgi ribbon organization highlighting the extended continuity of stacked Golgi cisternae. (C) Model clockwise rotated −120° about the vertical axis, and (D) Trapped budding profiles together with ‘free’ vesicles in the region displayed. For abbreviations and color scheme see Fig. 4. (E) Vesicles and arrested budding structures were assigned as clathrin- or COPI-coated profiles on the basis of their electron dense staining and diameters determined from a sphere fitted to the profile. Bar, 0.5 μm (A–D).

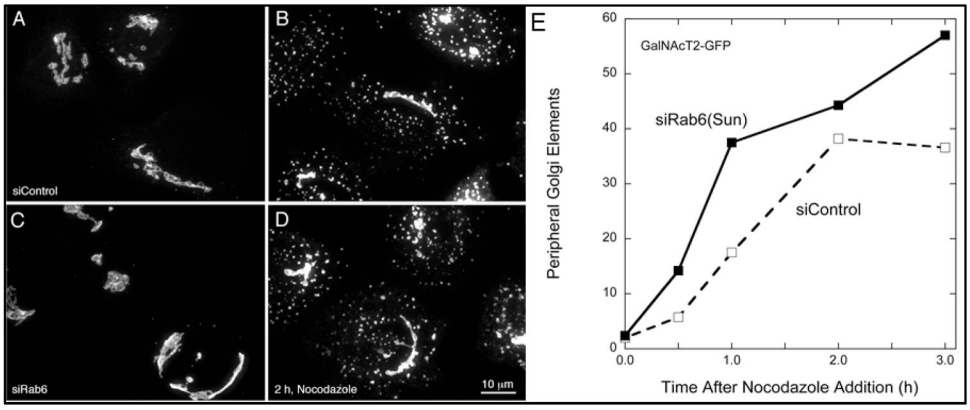

Fig. 6. The Golgi in Rab6-depleted HeLa cells remains sensitive to nocodazole-induced microtubule depolymerization

GalNAcT2-GFP HeLa cells incubated with either scrambled (siControl, A and B) or Rab6 siRNA (siRab6, C and D) for 96 h were either fixed immediately or treated with nocodazole at 10 μM for various time periods to depolymerize the microtubule cytoskeleton. Since we have shown that the fragmentation of the Golgi ribbon in response to microtubule polymerization is slow (54,56), an intermediate (i.e. 2 h) time point is presented to capture the Golgi ribbon prior to complete disassembly. Qualitatively, the punctate Golgi-derived elements induced by nocodazole-treatment appeared somewhat larger in siRab6-treated cells compared to controls. The kinetic incidence of peripheral Golgi elements (E) was computer scored as described in Materials and Methods. Bar, 10 μm (A–D).

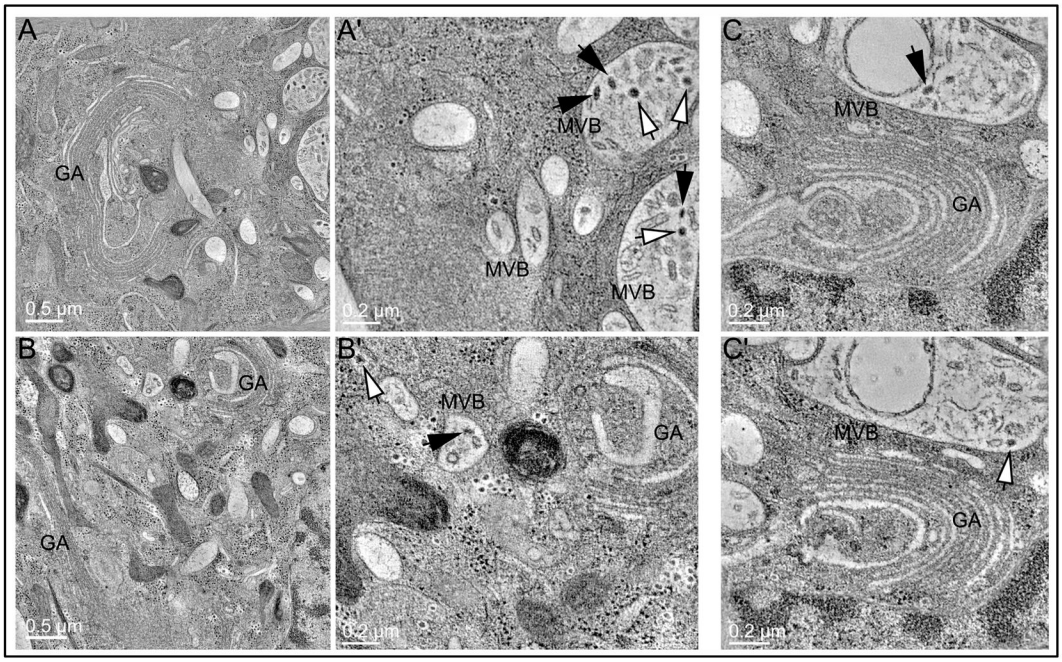

Fig. 7. The formation of multivesicular bodies/autophagic compartments is upregulated in Rab6-depleted cells

(A and B) Tomograms show the formation of extended endo-membrane compartments containing multiple/internal membranes and abundant coated vesicle profiles. (A′ and B′) Higher magnification views neighboring the Golgi clearly demonstrate two predominant types of coated vesicle profiles within the lumen associated with internalized membranes (black arrow versus white arrow). (C and C′) Image slices corresponding to different Z planes in the tomographic volume of a different Golgi region; coated budding profiles arrested in a ‘pre-scission’ state (C, black arrow) are evident, along with multiple ‘free’ coated vesicles (C′, white arrow). MVB, multivesicular body.

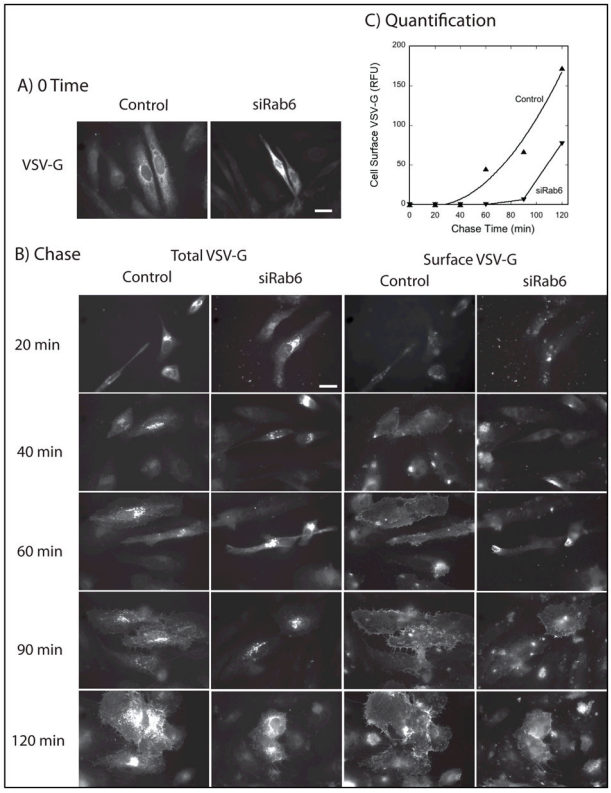

Fig. 8. Depletion of Rab6 inhibits VSV-G transport Golgi to cell surface, but not from the ER to Golgi apparatus

Wild-type HeLa cells were either incubated with Control or Rab6 (Sun) siRNAs for 4 d and then microinjected with plasmids encoding GFP tagged VSV-G protein. At the end of the expression period at 39.5°C, VSV-G protein was located in the ER by wide field light microscopy, 63x/1.40 numerical aperture objective (A, 0 time). Cells were then shifted to permissive conditions, 32°C, and fixed at various chase times (B). At the end of a 20 min chase, there was significant juxtanuclear, i.e., Golgi, accumulation of VSV-G protein in both Control and siRab6 cells (total VSV-G, left hand 2 columns). There was no quantitatively significant cell surface accumulation (Surface VSV-G, right hand 2 columns and Fig. 8C). At later chase times, cell surface accumulation was obvious qualitatively and quantitatively much earlier for Control than siRab6 cells. Rab6 cells were confirmed to be depleted for Rab6 protein by antibody staining. Scale bars in wide field images shown in A and B equal 20 μm.

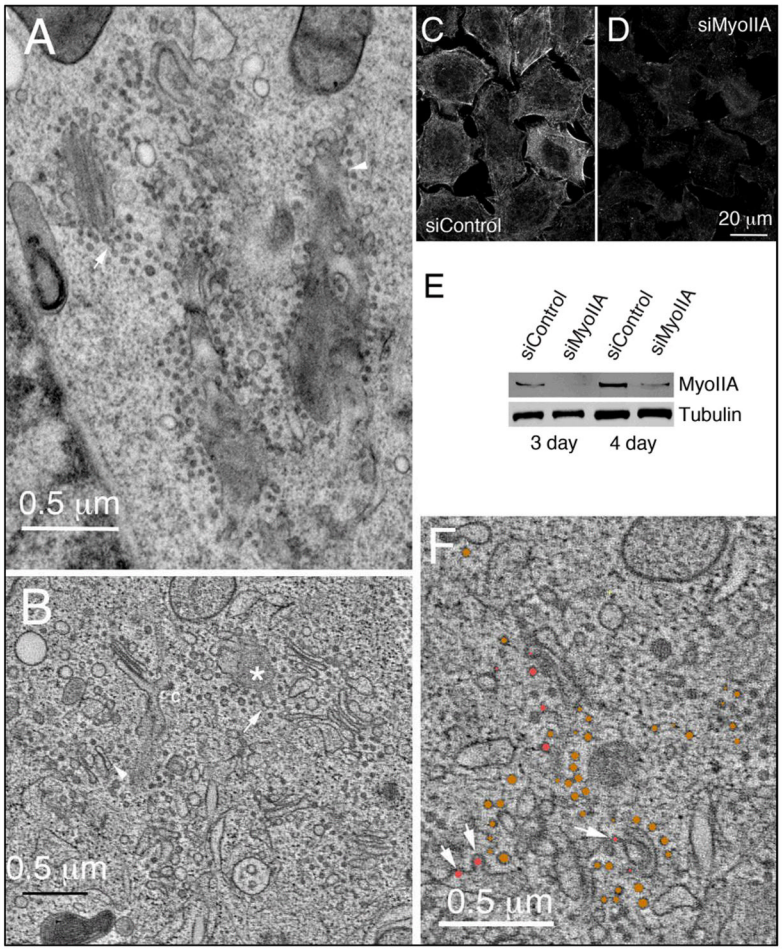

Fig. 9. Small uncoated Golgi-associated vesicles and tubules accumulate with selective depletion of the Rab6-effector MyoIIA indicating the specificity of the Rab6-knockdown Golgi phenotype

(A) Thin section electron micrograph of the Golgi region in a MyoIIA-depleted HeLa cell. Arrow points to an example of beads-on-a-string set of vesicles and a membrane-linked, stalked vesicle. (B) Tomogram of the Golgi region in a MyoIIA-depleted cell. Arrow and arrowheads point to examples as above. Asterisk marks an en face structure from which tubular elements appear to be extending. (C and D) Immunofluorescence (4 d) and (E) Western blot analysis for strong MyoIIA depletion with siRNA treatment. (F) Tomogram example showing apparent stages in formation of small arrested budding structures (arrows, rose color circles) in MyoIIA-depleted HeLa cell. Rose and bronze colored structures indicate budding or nearly fully released vesicles that were diameter quantified in Table 2. Bars, 10 μm (A, B, and F); 20 μm (C and D).

Table 1

Quantification of Golgi cisternae in siControl and siRab6 GaINAcT2-GFP HeLa

siControl Golgi		Maximum Cisterna Length (nm)/Longest Cisterna	Average Golgi Stack Width (nm)	Number of Cisternae per Stack	Number of Lateral Budding Structures?
Cell#	Stack #				
1	1	646.79/2nd medial	327.32	3	0
	2	648.76/ *trans*	240.21	5	0
	3	506.36/3rd medial	268.83	4	0
2	1	345.04/3rd medial	169.40	3	0
	2	761.12/3rd medial	345.18	5	0
	3	911.96/ *cis*	180.10	4	1
	4	630.35/2nd medial	279.58	4	0
	5	373.10/ *trans*	178.81	4	0
	6	385.74/1st medial	297.59	3	0
	7	704.12/ *trans*	149.22	3	0
3 Serial Section 1	1	334.53/2nd medial	167.38	4	0
	2	1005.66/1st medial	210.38	4	0
	3	793.15/ *trans*	157.24	3	0
	4	528.46/1st medial	279.85	3	0
3 Serial Section 2	1	352.82/2nd medial	156.41	4	0
	2	1062.50/1st medial	187.28	4	0
	3	837.71/ *trans*	169.68	3	0
	4	595.48/1st medial	280.26	3	0
Averages ± SEM		634.65±54.18 nm	224.21 ±15.3 nm	3.71 ±0.19	0.05±0.05

siRab6 Golgi		Maximum Cisterna Length (nm)/Longest Cisterna	Average Golgi Stack Width (nm)	Number of Cisternae per Stack	Number of Lateral Budding Structures
Cell#	Stack #				
1	1	5936.28/1st medial	323.21	7	12
2	1	1290.63/ 5th medial	267.41	7	0
3	1	1424.32/ *trans*	194.03	4	3

siRab6 Golgi		Maximum Cisterna Length (nm)/Longest Cisterna	Average Golgi Stack Width (nm)	Number of Cisternae per Stack	Number of Lateral Budding Structures
Cell#	Stack #				
	2	1714.32/1st medial	176.75	5	2
	3	N/A off screen	218.71	5	3
4	1	598.57/4th medial	372.57	6	3
	2	2166.79/2nd medial	437.98	5	5
	3	880.86/ 3rd medial	247.52	5	0
	4	1480.74/2nd medial	391.22	4	4
	5	N/A off screen	374.33	6	1
5	1	2248.18/ 5th medial	300.50	7	6
	2	2278.43/4th medial	189.15	6	8
Averages ± SEM		2001.9 ± 472 nm	291.1 ± 25.6 nm	5.6 ± 0.3	3.9 ± 1.00

Table 2

QUANTIFICATION OF TOMOGRAM VESICLE PROFILES FROM MYOIIA KD

	Color Code:				**Bronze**			**Color Code: Rose**	
	Free Vesicle (diameter in nm)				**Linked String of Free Vesicles (diameter in nm)**	**Membrane Linked Vesicle (diameter in nm)**		**Budding Vesicle (diameter in nm)**	
	55.4	40.3	34.0	41.6		40.3	36.5	59.2	46.6
	37.8	40.3	35.3	47.9		40.3	39.0	30.2	49.1
	26.5	39.0	45.3			36.5	37.8	37.8	61.7
	40.3	37.8	39.0			32.8	36.5	46.6	47.9
	36.5	36.5	35.3		(29.0, 32.8, 32.8, 34.0, 35.3, 31.5, 32.8, 30.2, 31.5, 32.8) avg: 32.2	32.8	40.3	27.7	32.8
	36.5	34.0	36.5			37.8	47.9	47.9	44.1
	32.8	47.9	37.8			32.8	32.8	42.8	46.6
	29.0	36.5	34.0			29.0	34.0	30.2	
	35.3	40.3	37.8			30.2		31.5	
	32.8	42.8	35.3			42.8		36.5	
	40.3	40.3	35.3		(29.0, 31.5, 34.0, 30.2, 35.3, 31.5, 31.5, 32.8, 34.0, 35.3, 29.0, 30.2, 31.5) avg: 30.6	29.0		34.0	
	39.0	41.6	37.8			29.0		37.8	
	37.8	36.5	26.5			32.8		32.8	
	39.0	40.3	36.5			35.3		41.6	
	36.5	29.0	42.8			30.2		42.8	
	41.6	32.8	37.8		(35.3, 52.9, 32.8, 34.0, 44.1, 34.0, 37.8, 40.3, 35.3, 37.8) avg: 38.4	35.3		50.4	
	37.8	45.3	36.5			37.8		49.1	
	50.4	378	44.1			34.0		34.0	
	50.4	34.0	46.6		(34.0, 37.8, 35.3, 29.0, 32.8, 50.4, 27.7, 26.5, 31.5, 29.0,39.0, 41.6, 32.8, 34.0, 29.0,	32.8		37.8	
	31.5	47.9	41.6		37.8,45.3) avg: 35.5	44.1		34.0	
	49.1	41.6	39.0			36.5		50.4	
	37.8	39.0	32.8			42.8		37.8	
	44.1	42.8	34.0			39.0		39.0	
	40.3	40.3	32.8			40.3		35.3	
	44.1	34.0	31.5		(30.2, 26.5, 32.8, 30.2, 30.2, 41.6, 30.2, 25.2, 36.5, 37.8,37.8, 34.0, 30.2, 26.5, 41.6, 37.8, 27.7, 29.0) avg: 32.5	*37.8*		37.8	
	36.5	35.3	49.1		(37.8, 39.0, 40.3, 35.3, 30.2, 27.7, 29.0, 31.5, 29.0, 30.2,32.8, 31.5, 35.3, 30.2, 26.5, 29.0, 27.7, 27.7, 32.8, 34.0) avg: 31.5	34.0		31.5	

	Color Code:				Bronze			Color Code: Rose		
	Free Vesicle (diameter in nm)				Linked String of Free Vesicles (diameter in nm)			Membrane Linked Vesicle (diameter in nm)		Budding Vesicle (diameter in nm)	
	31.5	34.0	45.3					40.3		42.8	
	41.6	51.7	30.2					35.3		34.0	
	41.6	44.1	35.3					31.5		26.4	
	37.8	41.6	32.8					35.3		46.6	
Count	92 (36% of total vesicles)				88 (34%)			38 (15%)		37(15%	
Avg ± SEM	42.4 ± 3.73 nm				33.5 ± 0.5 nm			36.1 ± 0.7 nm		40.4 ± 1.4 nm	
Range	26.5–55.4 nm				29.0–52.9 nm			29.0–42.8 nm		26.4–61.7 nm	

The color-coding into rose and bronze colored structures indicate classifications of budding or nearly fully released vesicles that are illustrated fully in the Figure 9 tomogram. A total of 255 profiles were scored.

Table 3

QUANTIFICATION OF GOLGI CISTERNAE OF MYOIIA KNOCKDOWN GOLGI

MyoIIA Depleted Golgi Apparatus		Maximum Cisterna Length (nm)/Longest Cisterna	Average Golgi Stack Width (nm)	Number Cisternae per Stack	Number of Transverse Budding Structures
	Stack #				
	1	443.92/ *cis*	140.99	3	0
	2	1222.31/1st medial	206.90	3	1
	3	365.50/ *cis*	75.79	2	1
	4	321.50/*trans*	78.67	2	0
	5	507.83/ *trans*	160.92	3	0
	6	400.55/ *cis*	173.19	3	0
	7	317.74/ *cis*	105.61	3	0
Averages ± SEM		511 ± 121 nm	135 ± 19 nm	2.71 ± 0.18	0.29 ± 0.2